Università degli Studi di Padova

DIPARTIMENTO DI INGEGNERIA DELL'INFORMAZIONE

Università degli Studi di Padova

Dipartimento di Ingegneria dell'Informazione

Corso di Laurea in
Ingegneria dell'Informazione

Theory and implementation of Quantum Computing

Relatore:
Prof. Giuseppe Vallone

Laureando:
Nicola Basso
1162661

Anno Accademico 2022/2023

Abstract

This paper gives the reader an overview on the physics behind quantum computing, introducing basic concepts like qubit and gates. Then it shows two of the most prevalent implementation: Ion Trap Quantum Computer and Superconducting Quantum Computer.

Contents

Chapter 1

The theory behind quantum computing

1.1 The Qubit

The elementary unit of quantum information is the qubit. A single qubit can be envisaged as a 2-state system described by a two-dimensional complex Hilbert space. A quantum system is said to have n qubits if it has a Hilbert space of $2n$ dimensions and so has available 2^n mutually orthogonal quantum states (recall that n classical bits can represent up to 2^n different things). We will write two orthogonal states of a single qubit as

$$\{|0\rangle, |1\rangle\}. \tag{1.1}$$

More generally, 2^n mutually orthogonal states of n qubits can be written

$$\{|i\rangle\}, \tag{1.2}$$

where i is an n bit binary number. For example, for three qubits we have

$$\{|000\rangle\ ,\ |001\rangle\ ,\ |010\rangle\ ,\ |011\rangle\ ,\ |100\rangle\ ,\ |101\rangle\ ,\ |110\rangle\ ,\ |111\rangle\}. \tag{1.3}$$

The superposition principle shows that the state of a qubit can be written as

$$|\psi\rangle = \alpha|0\rangle + \beta|1\rangle, \tag{1.4}$$

where α and β are complex numbers that respect the normaliziation condition

$$|\alpha|^2 + |\beta|^2 = 1, \tag{1.5}$$

The generic state of a qubit may be written as

$$|\psi\rangle = \cos\frac{\theta}{2}|0\rangle + \mathrm{e}^{i\phi}\sin\frac{\theta}{2}|1\rangle \tag{1.6}$$

$$= \begin{bmatrix} \cos\frac{\theta}{2} \\ \mathrm{e}^{i\phi}\sin\frac{\theta}{2} \end{bmatrix} \tag{1.7}$$

Therefore, unlike the classical bit, which can only be set equal to 0 or 1, the qubit resides in a vector space, parametrized by the continuous variables α and β (or θ and ϕ). Thus, a continuum of states is allowed.

A two-level quantum system can be used in practice as a qubit if it is possible to manipulate it as follows:

(i) it can be prepared in some well-defined state, for example the state $|0\rangle$, which we call the fiducial state of the qubit;

(ii) any state of the qubit can be transformed into any other state. Such transformations are carried out by means of unitary transformations;

(iii) the qubit state can be measured in the computational basis $|0\rangle$, $|1\rangle$. This means that we can measure the qubit polarization along the z-axis. the Hermitian operator associated with this measurement is the Pauli operator σ_z, which has eigenstates $|0\rangle$ and $|1\rangle$. Now, if the state of the qubit is described by Eq. (1.7), as a result of the measurement one obtains 0 or 1 with probabilities

$$p_0 = |\langle 0|\psi\rangle|^2 = \cos\frac{\theta}{2}^2, \quad p_1 = |\langle 1|\psi\rangle|^2 = \sin\frac{\theta}{2}^2 \tag{1.8}$$

which have been computed using Postulate II of quantum mechanics

1.2 The Bloch Shere

The Bloch sphere is a simple way to provide a geometric rapresentation of a qubit. The north and south poles of the Bloch sphere are typically chosen to correspond to the standard basis vectors $|0\rangle$ and $|1\rangle$, respectively. This choice is arbitrary, however. The points on the surface of the sphere correspond to the

pure states of the system, whereas the interior points correspond to the mixed states. The Bloch sphere may be generalized to an n-level quantum system, but then the visualization is less useful. Given an orthonormal basis, any pure state of a two-level quantum system can be written as a superposition of the basis vectors and, where the coefficient of (or contribution from) each of the two basis vectors is a complex number. This means that the state is described by four real numbers. However only the relative phase between the coefficients of the two basis vectors has any physical meaning (the phase of the quantum system is not directly measurable), so that there is redundancy in this description. We can take the coefficient of $|0\rangle$ to be real and non-negative. This allows the state to be described by only three real numbers, giving rise to the three dimensions of the Bloch sphere. Owing to the notrmalization condition

$$\langle\psi|\psi\rangle = \|\psi\|^2 = 1 \tag{1.9}$$

Given this constraint, we can write $|\psi\rangle$ using the following representation:

$$|\psi\rangle = \cos\frac{\theta}{2}\,|0\rangle + \mathrm{e}^{i\phi}\sin\frac{\theta}{2}\,|1\rangle, \tag{1.10}$$

where $0 \leq \theta \leq \pi$ and $0 \leq \phi < 2\pi$.
The parameters θ and ϕ can be interpreted in spherical coordinates as the colatitude with respect to the z-axis and the longitude with respect to the x-axis, this way they specify a point

$$\vec{a} = (\sin\theta\cos\phi,\ \sin\theta\sin\phi,\ \cos\theta) = (u, v, w) \tag{1.11}$$

on the unit sphere in $\mathbb{R}^3$. Now the Eq.1.7 can be written as

$$|\psi\rangle = \begin{bmatrix} \sqrt{\frac{1+z}{2}} \\ \frac{x+iy}{\sqrt{2(1+z)}}. \end{bmatrix} \tag{1.12}$$

Anotheru usefull rapresentation of the state 1.7 is obtained using a projector $P = |\psi\rangle\langle\psi|$. The matrix of P in the basis $|0\rangle, |1\rangle$ is given by

$$P = \begin{bmatrix} \cos^2\frac{\theta}{2} & e^{-i\phi}\sin\frac{\theta}{2}\cos\frac{\theta}{2} \\ e^{i\phi}\sin\frac{\theta}{2}\cos\frac{\theta}{2} & \sin^2\frac{\theta}{2} \end{bmatrix} \tag{1.13}$$

$$= \frac{1}{2}\begin{bmatrix} 1+z & x-iy \\ x+iy & 1-z \end{bmatrix} \tag{1.14}$$

where the matrix element $P_{ij}(i, j = 0, 1)$ is defined as $\langle i|P|j\rangle$.

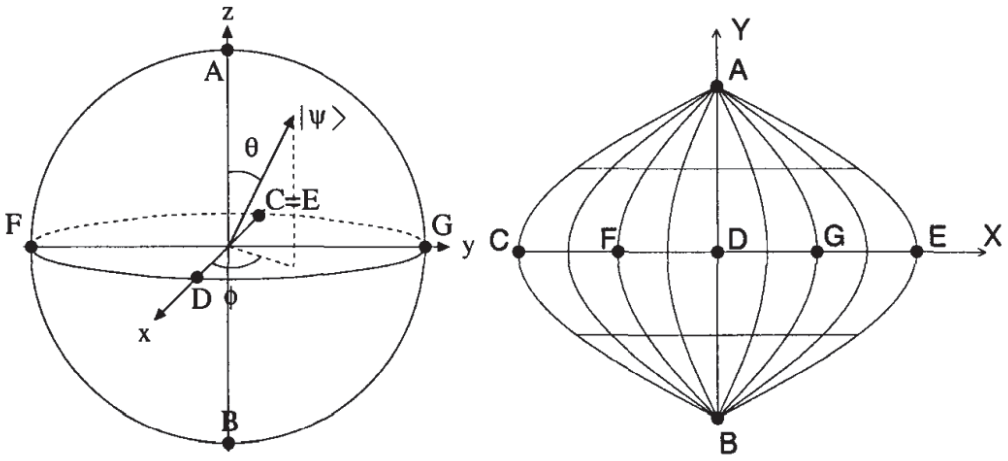

Figure 1.1: Bloch-sphere representation of a qubit (left) and sinusoidal projection of the Bloch sphere (right). The points corresponding to the following states are shown: $A = (\alpha = 1, \beta = 0)$,$B = (0, l)$, $C = E = (\frac{1}{\sqrt{2}}, -\frac{1}{\sqrt{2}})$, $D = (\frac{1}{\sqrt{2}}, \frac{1}{\sqrt{2}})$, $F = (\frac{1}{\sqrt{2}}, -\frac{1}{\sqrt{2}})$,and $G = (\frac{1}{\sqrt{2}}, \frac{1}{\sqrt{2}})$. Note that the points A (north pole of the Bloch sphere) and B (south pole) correspond to the states $|0\rangle and|1\rangle$, respectively.

1.3 Measuring the State of a Qubit

The state $\psi\rangle = \alpha|0\rangle + \beta|1\rangle$ of a qubit can be measured in principle, provided we measure a sufficiently large number of identically prepared qubits. With the Bloch-sphere rapresentation as a framework we shall show that the coordinates x, y and z of a qubit on the Bloch sphere can be measured. Using the Pauli operators, written in the computational basis as

$$\sigma_x = \begin{bmatrix} 0 & 1 \\ 1 & 0 \end{bmatrix},\ \sigma_y = \begin{bmatrix} 0 & -i \\ i & 0 \end{bmatrix},\ \sigma_z = \begin{bmatrix} 1 & 0 \\ 0 & -1 \end{bmatrix}, \tag{1.15}$$

one has, for the state $|\psi\rangle$ given by Eq.1.7

$$\begin{aligned}
\sigma_x|\psi\rangle &= \mathrm{e}^{i\phi}\sin\tfrac{\theta}{2}\,|0\rangle + \cos\tfrac{\theta}{2}\,|1\rangle \\
\sigma_y|\psi\rangle &= -i\mathrm{e}^{i\phi}\sin\tfrac{\theta}{2}\,|0\rangle + \cos\tfrac{\theta}{2}\,|1\rangle \\
\sigma_z|\psi\rangle &= \sin\tfrac{\theta}{2}\,|0\rangle - \mathrm{e}^{i\phi}\cos\tfrac{\theta}{2}\,|1\rangle
\end{aligned} \tag{1.16}$$

Consequently, the following expectation values for the state1.7 are obtained:

$$\begin{aligned}
\langle\psi|\sigma_x|\psi\rangle &= \langle\psi|\begin{bmatrix} 0 & 1 \\ 1 & 0 \end{bmatrix}|\psi\rangle = \sin\theta\cos\phi = x \\
\langle\psi|\sigma_y|\psi\rangle &= \langle\psi|\begin{bmatrix} 0 & -i \\ i & 0 \end{bmatrix}|\psi\rangle = \sin\theta\sin\phi = y \\
\langle\psi|\sigma_z|\psi\rangle &= \langle\psi|\begin{bmatrix} 1 & 0 \\ 0 & -1 \end{bmatrix}|\psi\rangle = \cos\theta = z
\end{aligned} \tag{1.17}$$

The coordinates (x, y, z) can be obtained with arbitrary accuracy by projection on the computational basis, that is, measuring σ_z. Indeed, from Eq.(1.8) we obtain

$$p_0 - p_1 = \cos^2\tfrac{\theta}{2} - \sin^2\tfrac{\theta}{2} = \cos\theta = z \tag{1.18}$$

In this way the coordinate z is given by the difference of the probabilities to obtain outcomes 0 or 1 from a measurement of σ_z.
If we have at our disposal a large number N of systems identically prepared in the state (1.7), we can estimate z as $N_0/N - N_i/N$, where N_0 and N_i count the number of outcomes 0 and 1. Therefore, z can be measured to any required accuracy, provided we measure a sufficiently large number of states. The coordinates x and y can be obtained by operating a unitary transformation on the qubit. If the unitary transformation described by the matrix

$$U_1 = \frac{1}{\sqrt{2}}\begin{bmatrix} 1 & 1 \\ -1 & 1 \end{bmatrix} \tag{1.19}$$

is applied to the state 1.7, we obtain the state $|\psi^{(1)}\rangle = U_1|\psi\rangle$. A projection on the computational basis then gives outcome 0 or 1 with probabilities $p_0^{(1)} = |\langle 0|\psi^{(1)}\rangle|^2$ and $p_1^{(1)} = |\langle 1|\psi^{(1)}\rangle|^2$, respectively. Therefore, we obtain

$$p_0^{(1)} - p_1^{(1)} = \cos\phi\sin\theta = x \tag{1.20}$$

In the same way, if the state (1.7) is transformed by means of the matrix

$$U_2 = \frac{1}{\sqrt{2}} \begin{bmatrix} 1 & -i \\ -i & 1 \end{bmatrix} \tag{1.21}$$

we obtain the state $|\psi^{(2)}\rangle = U_2|\psi\rangle$. Therefore,

$$p_0^{(2)} - p_1^{(2)} = \sin\phi \sin\theta = y \tag{1.22}$$

where $p_0^{(2)} = |\langle 0|\psi^{(2)}\rangle|^2$ and $p_1^{(2)} = |\langle 1|\psi^{(2)}\rangle|^2$ give the probabilities to obtain outcome 0 or 1 from the measurement of the qubit polarization along z.

1.4 Circuit Model of quantum computing

A classical computer can be described in simple terms as a finite register of n bits. A combination of elementary operation, such as NOT or AND, can produce any given logic function. The circuit model can be transferred to quantum computation. The quantum computer can be thought of as a finite collection of n qubits. While the state of a classical computer is described by a binary integer $i \in [0, 2^n - 1]$,

$$i = i_{n-1}2^{n-1} + \cdots + i_1 2 + i_0, \tag{1.23}$$

with i_0,i_1,...,$i_{n-1} \in [0, 1]$ binary digits, the state of a quantum computer is

$$\begin{aligned} |\psi\rangle &= \sum_{i=0}^{2^n-1} c_i |i\rangle \\ &= \sum_{i_{n-1}=0}^{1} \cdots \sum_{i_1=0}^{1} \sum_{i_0=0}^{1} c_{i_{n-1},\ldots,i_1,i_0} |i_{n-1}\rangle \otimes \cdots \otimes |i_1\rangle \otimes |i_0\rangle, \end{aligned} \tag{1.24}$$

with the complex numbers c_i constrained by the normalization condition

$$\sum_{i=0}^{2^{n-1}} |c_i|^2 = 1. \tag{1.25}$$

Therefore the state of a quantum computer is a wave function residing in a 2^n dimensional Hilbert space constructed as the tensor product of n 2-dimensional Hilbert spaces, one for each qubit. For example, considering a quantum computer

with $n = 2$ qubit, we can write its generic state as

$$\begin{aligned}|\psi\rangle &= c_0|0\rangle + c_1|1\rangle + c_2|2\rangle + c_3|3\rangle \\ &= c_{0,0}|0\rangle \otimes |0\rangle + c_{0,1}|0\rangle \otimes |1\rangle + c_{1,0}|1\rangle \otimes |0\rangle + c_{1,1}|1\rangle \otimes |1\rangle \\ &= c_{00}|00\rangle + c_{01}|01\rangle + c_{10}|10\rangle + c_{11}|11\rangle, \end{aligned} \tag{1.26}$$

where in (1.26) we have used the shorthand notation $|i_0 i_1\rangle = |i_1\rangle \otimes |i_0\rangle$. The same can be done for (1.24) which can be written as

$$|\psi\rangle = \sum_{i_{n-1},\ldots,i_1,i_0=0}^{1} c_{i_{n_1}\ldots i_1 i_0}|i_{n-1}\ldots i_1 i_0\rangle. \tag{1.27}$$

The superposition principle is visible in Eq. (1.24): while n classical bits can store only a single integer i, the n-qubit quantum register can be prepared in the corresponding state $|i\rangle$ of the computational basis, but also in a superposition. The superposition allows to store as many as 2^n different states of the computational basis, a number which grows exponentially with the number of qubits. In a classical computer different inputs require separate run to yield a result, in contrast, a quantum computer can perform a computation for exponentially many inputs on a single run. This parallelism is the basis of the power of quantum computing. There are 3 requirements in order to perform a quantum computation:

(i) prepare the quantum computer in a well-defined initial state $|\psi_i\rangle$, which we call the fiducial state of the computer, for example $|00\rangle$;

(ii) manipulate the quantum-computer wave function, this can be done by executing a unitary transformation U on a single qubit to change its state, for instance moving $|\psi\rangle$ to a new state $|\psi_f\rangle = U|\psi_i\rangle$

(iii) perform a standard measurement in the computational basis on the result of the computation, that is, measure the polarization σ_z of each qubit.

1.5 Single-qubit gates

The operations on a qubit must preserve the normalization condition and are thus described by 2×2 unitary matrices [2].

The Hadamard gate

The Hadamard gate acts on a sigle qubit. It maps the basis state $|0\rangle \mapsto \frac{|0\rangle+|1\rangle}{\sqrt{2}}$ and $|1\rangle \mapsto \frac{|0\rangle-|1\rangle}{\sqrt{2}}$. The two states are sometimes written as $|+\rangle$ and $|-\rangle$ respectively. The Hadamard gate performs a rotation of π about the axis $(\hat{x}+\hat{z})/\sqrt{2}$ at the Bloch sphere. It is rapresented by the Hadamard matrix:

Figure 1.2: Hadamard gate

$$H = \frac{1}{\sqrt{2}}\begin{bmatrix} 1 & 1 \\ 1 & -1 \end{bmatrix} \tag{1.28}$$

The Hadamard gate is hermitian, meaning $H^\dagger = H^{-1} = H$. This gate is used to perform a change of basis, it flips $\hat{x}$ and $\hat{z}$. For example, $HZH = X$.

The Phase Shift gate

The phase shift is a single-qubit gate that maps the basis states $|0\rangle \mapsto |0\rangle$ and $|1\rangle \mapsto e^{i\varphi}|1\rangle$. The probability of measuring a $|0\rangle$ or $|1\rangle$ is unchanged after applying this gate, however it modifies the phase of the quantum state. This is equivalent to tracing a horizontal circle (a line of latitude), or a rotation along the z-axis on the Bloch sphere by φ radians. The phase shift gate is represented by the matrix:

$$P(\varphi) = \begin{bmatrix} 1 & 0 \\ 0 & \mathrm{e}^{i\varphi} \end{bmatrix} \tag{1.29}$$

where φ is the phase shift with the period 2π. Some common examples are the T gate where $\varphi = \frac{\pi}{4}$, the phase gate (also known as the S gate) where $\varphi = \frac{\pi}{2}$ and the Pauli-Z gate where $\varphi = \pi$. The action of a phase-shift gate on a generic single-qubit state $|\psi\rangle$, gives

$$R_z(\varphi)|\psi\rangle = \begin{bmatrix} 1 & 0 \\ 0 & \mathrm{e}^{i\varphi} \end{bmatrix}\begin{bmatrix} \cos\frac{\theta}{2} \\ \mathrm{e}^{i\phi}\sin\frac{\theta}{2} \end{bmatrix} = \begin{bmatrix} \cos\frac{\theta}{2} \\ \mathrm{e}^{i(\phi+\varphi)}\sin\frac{\theta}{2}. \end{bmatrix} \tag{1.30}$$

it is easy to recognize that this gate performs a counterclockwise rotation through an angle delta about the z axis of the Bloch Sphere

Using this two gates one can perform any unitary operation on a single qubit. For example we can move from a state 1 parametrized on the bloch sphere by the angles (θ_1, ϕ_1) into the state (θ_2, ϕ_2) using the unitary operator

$$R_z(\frac{\pi}{2}+\phi_2)HR_z(\theta_2-\theta_1)HR_z(-\frac{\pi}{2}-\phi_1). \tag{1.31}$$

1.6 Controlled gates and entanglement generation

Entanglement, which is the most intriguing characteristic of quantum mechanics, appears already with two qubits. Actually, a generic two-qubit state can be written in the computational basis as

$$|\psi\rangle = \alpha|00\rangle + \beta|01\rangle + \gamma|10\rangle + \delta|11\rangle, \tag{1.32}$$

with α, β, γ and δ complex coefficients. Taking into account the normalization condition, $\alpha|^2 + |\beta|^2 + |\gamma|^2 + |\delta|^2 = 1$ and the fact that the state is only defined up to an overall phase factor, there remain 6 real degrees of freedom. Therefore the state (1.32) is not separable and can be classified as such only if written as the tensor product of n qubits with defined state. For example a 2-qubit state $|\psi\rangle$ is separable if written as $|\psi\rangle = |\psi_1\rangle \otimes |\psi_2\rangle$. Only in this case the resulting 2-qubit state has just 4 degrees of freedom since we can take for each qubit the two parameters of its Bloch Sphere. The complexity of entanglement grows exponentially with the number of qubits: while a separable state of n qubits depends only on 2^n real parameters, the most general entangled state has $2(2^n|1)$ degrees of freedom. It is clear that single-qubit gates are unable to generate entanglement in an n-qubit system. Since they operate on every qubit individually, the resulting n-qubit state is still separable. To create an entangled state one needs inner-qubit operations witch can be obtained using a two-qubit gate.

The controlled-NOT gate

A useful example of two-qubit gate is the controlled-NOT gate or CNOT. It performs the NOT operation on the second qubit only when the first qubit is $|1\rangle$, and otherwise leaves it unchanged. Using the basis $|00\rangle$, $|01\rangle$, $|10\rangle$, $|11\rangle$, it can be represented by the Hermitian unitary matrix:

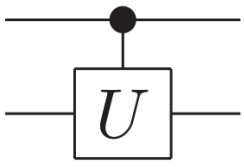

Figure 1.3:
controlled-NOT gate

$$CNOT = \begin{bmatrix} 1 & 0 & 0 & 0 \\ 0 & 1 & 0 & 0 \\ 0 & 0 & 0 & 1 \\ 0 & 0 & 1 & 0 \end{bmatrix} \tag{1.33}$$

where the components $(CNOT)_{ij}$ of this matrix are given by $(CNOT)_{ij} = \langle i|CNOT|j\rangle$. The CNOT gate can be described as the gate that maps the basis states $|a,b\rangle \mapsto |a, a \otimes b\rangle$, where $\otimes$ is the XOR logic operator. Note that the CNOT gate is self-inverse, since $(CNOT)^2 = I$. It is easy to show that CNOT can generate entanglement. For exampele,

$$CNOT(\alpha|0\rangle + \beta|1\rangle)|0\rangle = \alpha|00\rangle + \beta|11\rangle, \tag{1.34}$$

which is non-separable insofar as $\alpha, \beta \neq 0$.

The SWAP gate

The SWAP gate swaps two qubits. Using the basis $|00\rangle$,$|01\rangle$,$|10\rangle$,$|11\rangle$, it can be represented by the matrix:

$$SWAP = \begin{bmatrix} 1 & 0 & 0 & 0 \\ 0 & 0 & 1 & 0 \\ 0 & 0 & 1 & 0 \\ 0 & 0 & 0 & 1 \end{bmatrix}. \tag{1.35}$$

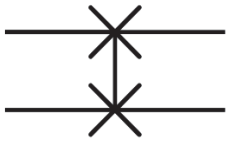

Figure 1.4: SWAP gate

The swap gate can be decomposed into summation form:

$$SWAP = \frac{I \otimes I + X \otimes X + Y \otimes Y + Z \otimes Z}{2} \tag{1.36}$$

The Toffoli gate

The Toffoli gate also colled CCNOT gate or Deutsch gate $D(\pi/2)$, is a 3-qubit gate which is universal for classical computation but not for quantum computation. The Toffoli gate is similar to controlled-NOT gate except for the number of input qubits. Accepting input qubits that are either $|0\rangle$ or $|1\rangle$, it executes the NOT operation on the third qubit if the first two bits are in the state $|1\rangle$, else it does nothing. The Toffoli gate is related to the classical AND and XOR operations as it performs the mapping $|a,b,c\rangle \mapsto |a,b,c\oplus(a\wedge b)$ on states in the computational basis. Finally the Toffoli gate can be part a universal set of gates when combined with the single qubit Hadamand gate.

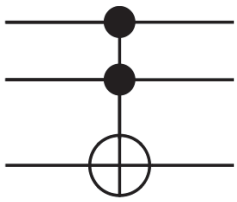

Figure 1.5: Toffoli gate

1.7 The bell basis

A common application of the $CNOT$ gate is to maximally entangle two qubits into the Bell state; this forms part of the setup of the superdense coding, quantum teleportation, and entangled quantum cryptography algorithms. The bell basis is defined by [2]

$$|\Psi^+\rangle = \frac{1}{\sqrt{2}}(|0\rangle_A \otimes |0\rangle_B + |1\rangle_A \otimes |1\rangle_B) \tag{1.37}$$

$$|\Psi^-\rangle = \frac{1}{\sqrt{2}}(|0\rangle_A \otimes |0\rangle_B - |1\rangle_A \otimes |1\rangle_B) \tag{1.38}$$

$$|\Psi^+\rangle = \frac{1}{\sqrt{2}}(|0\rangle_A \otimes |1\rangle_B + |1\rangle_A \otimes |0\rangle_B) \tag{1.39}$$

$$|\Psi^-\rangle = \frac{1}{\sqrt{2}}(|0\rangle_A \otimes |1\rangle_B - |1\rangle_A \otimes |0\rangle_B) \tag{1.40}$$

Although there are many possible ways to create entangled Bell states through quantum circuits, the simplest takes a computational basis as the input and contain a Hadamard gate and a CNOT gate (1.6). The quantum circuit in picture takes the two qubit input $|00\rangle$ and transforms it into the first Bell state, Fig.1.37.

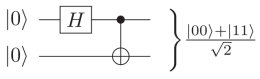

Figure 1.6: Quantum circuit to create the Bell state $|\Psi\rangle^+$.

1.8 Universal Quantum Gates

A set of universal quantum gates is a set of gates that can be used as building blocks to create any operation possible on a quantum computer, with this set any unitary operation can be expressed as a finite sequence of gates. The rotation operators $R_x(\theta)$, $R_y(\theta)$, $R_z(\theta)$, the phase shift gate $P(\phi)$ and $CNOT$ form a widely used universal set of quantum gates. $CNOT$, H, S and T make another common univerasal gate set referred as the Clofford + T gate set. The Toffoli gate forms a set of universal gates for reversible boolean algebraic logic circuits witch can be expanded to a two-gate set of universal quantum gates by adding the Hadamard gate to the set. The three-qubit Deutsch gate $D(\theta)$ can be used as a single-gate set of universal quantum gates. The Toffoli gate, a universal logic gate for reversible classical computing, can be reduced to a Deutsch gate $D(\pi/2)$, showing that all reversible classical logic operations can be performed on a universal quantum computer.

1.9 Circuit composition

Series gates

With two gates A and B, that both act on n qubits if B is put after A in a series circuit, then the effect of the two gates can be described as a single gate C.

$$A = B \cdot C \tag{1.41}$$

where $\cdot$ is matrix multiplication.

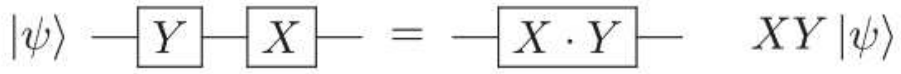

Figure 1.7: Two gates Y and X in series. The order in which they appear on the wire is reversed when multiplying them together.

Parallel gates

The tensor product of two quantum gates is the gate that is equal to the two gates in parallel. If we, as in the picture, combine the Pauli-Y gate with the

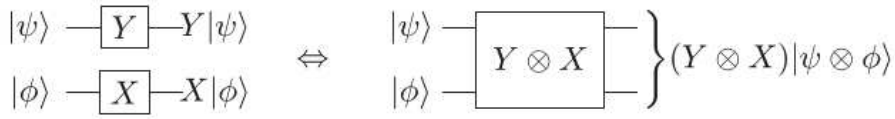

Figure 1.8: Two gates Y and X in parallel is equivalent to the gate $Y \otimes X$

Pauli-X gate in parallel, then this can be written as:

$$\begin{aligned} C &= Y \otimes X \\ &= \begin{bmatrix} 0 & -i \\ i & 0 \end{bmatrix} \otimes \begin{bmatrix} 0 & 1 \\ 1 & 0 \end{bmatrix} = \begin{bmatrix} 0\begin{bmatrix} 0 & 1 \\ 1 & 0 \end{bmatrix} & -i\begin{bmatrix} 0 & 1 \\ 1 & 0 \end{bmatrix} \\ i\begin{bmatrix} 0 & 1 \\ 1 & 0 \end{bmatrix} & 0\begin{bmatrix} 0 & 1 \\ 1 & 0 \end{bmatrix} \end{bmatrix} = \begin{bmatrix} 0 & 0 & 0 & -i \\ 0 & 0 & -i & 0 \\ 0 & i & 0 & 0 \\ i & 0 & 0 & 0 \end{bmatrix} \end{aligned} \tag{1.42}$$

Both the Pauli-X and the Pauli-Y gate act on a single qubit. The resulting gate acts on two qubits.

Hadamard transform

The gate $H_2 = H \otimes H$ is the Hadamard gate (H) applied in parallel on 2 qubits. It can be written as:

$$H_2 = H \otimes H = \frac{1}{\sqrt{2}} \begin{bmatrix} 1 & 1 \\ 1 & -1 \end{bmatrix} \otimes \frac{1}{\sqrt{2}} \begin{bmatrix} 1 & 1 \\ 1 & -1 \end{bmatrix} = \frac{1}{2} \begin{bmatrix} 1 & 1 & 1 & 1 \\ 1 & -1 & 1 & -1 \\ 1 & 1 & -1 & -1 \\ 1 & -1 & -1 & 1 \end{bmatrix} \tag{1.43}$$

This "two-qubit parallel Hadamard gate" will when applied to, for example, the two-qubit zero-vector ($|00\rangle$), create a quantum state that have equal probability of being observed in any of its four possible outcomes: $|00\rangle$, $|01\rangle$, $|10\rangle$, $|11\rangle$.

$$H_2|00\rangle = \frac{1}{2} \begin{bmatrix} 1 & 1 & 1 & 1 \\ 1 & -1 & 1 & -1 \\ 1 & 1 & -1 & -1 \\ 1 & -1 & -1 & 1 \end{bmatrix} \begin{bmatrix} 1 \\ 0 \\ 0 \\ 0 \end{bmatrix} = \frac{1}{2} \begin{bmatrix} 1 \\ 1 \\ 1 \\ 1 \end{bmatrix} = \frac{|00\rangle + |01\rangle + |10\rangle + |11\rangle}{2} \tag{1.44}$$

When applied to a register of n qubits all initialized to $|0\rangle$, the Hadamard transform puts the quantum register into a superposition with equal probability of being measured in any of its 2^n possible states. This state is a uniform superposition and it is generated as the first step in some search algorithms, for example in amplitude amplification and phase estimation.

Chapter 2

Ion Trap Quantum Computer

Electron and nuclear spins provide potentially good representations for qubits. Spin is a strange (but very real) concept, but since the energy difference between different spin states is typically very small compared with other energy scales (such as the kinetic energy of typical atoms at room temperature), the spin states of an atom are usually difficult to observe, and even more difficult to control. In carefully crafted environments, however, exquisite control is possible. Such circumstances are provided by isolating and trapping small numbers of charged atoms in electromagnetic traps, then cooling the atoms until their kinetic energy is much lower than the spin energy contribution. After doing this, incident monochromatic light can be tuned to selectively cause transitions which change certain spin states depending on other spin states. This is the essence of how trapped ions can be made to perform quantum computation. [2]

2.1 Physical Apparatus

The experimental apparatus is an electromagnetic trap constructed from four cylindrical electrodes (Fig.2.1). The end segments of the electrodes are biased at a different voltage U0 than the middle, so that the ions are axially confined by a static potential $\Phi_{dc} = \kappa U_0[z^2 - (x^2 + y^2)]/2$ along the $\hat{z}$ axis (κ is a geometrical factor). However, a result known as Earnshaw's theorem states that a charge cannot be confined in three dimensions by static potentials. Thus, to provide confinement, two of the electrodes are grounded, while the other two are driven by a fast oscillating voltage which creates a radiofrequency (RF) potential $\Phi_{rf} = (V_0 \cos \Theta_T t + U_r)(1 + (x^2 - y^2)/R^2)/2$, where R is a geometrical factor. The segments of the electrodes are capacitively coupled such that the RF potential is

constant across them. The combination of Φ_{dc} and Φ_{rf} creates, on average (over Ω_T), a harmonic potential in x, y, and z. Together with the Coulomb repulsion of the ions, this gives a Hamiltonian governing the motion of the N ions in the trap,

$$H = \sum_{i=1}^{N} \frac{M}{2}(\omega_x^2 x_i^2 + \omega_y^2 y_i^2 + \omega_z^2 z_i^2 + \frac{|\vec{p_i}|^2}{M^2}) + \sum_{i=1}^{N}\sum_{j>i} \frac{e^2}{4\pi\epsilon_0 |\vec{r_i} - \vec{r_j}|} \tag{2.1}$$

where M is the mass of each ion. Typically, ω_x, $\omega_y \gg \omega_z$ by design, so that the ions all lie generally along the $\hat{z}$ axis. As the number of ions becomes large, the geometrical configuration of the ions can become quite complicated, forming zig-zag and other patterns, but we shall focus on the simple case where just a few ions are trapped, in a string-like configuration.

Just as a mass on a spring can behave as a quantum system when the coupling

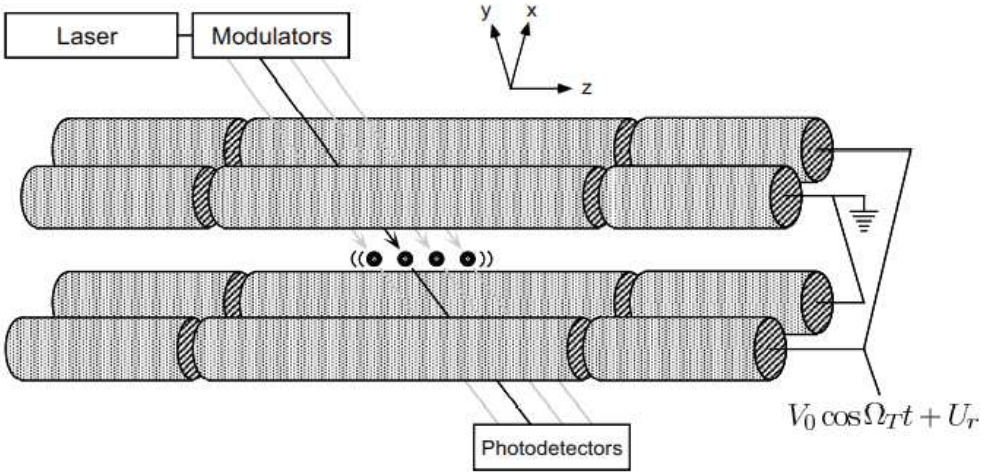

Figure 2.1: Schematic drawing (not to scale) of an ion trap quantum computer, depicting four ions trapped in the center of a potential created by four cylindrical electrodes. The apparatus is typically contained in a high vacuum (≈ 10-8 Pa), and the ions are loaded from a nearby oven. Modulated laser light incident on the ions through windows in vacuum chamber perform operations on and are used to readout the atomic states.

to the external world becomes sufficiently small, the motion of the electromagnetically confined ion becomes quantized when it is sufficiently well isolated. Let us first understand what the quantization means, then consider the isolation criteria. The energy levels of a harmonic oscillator are equally spaced, in units of ω_z. In the ion trap, in the regime which concerns us, these energy eigenstates represent different vibrational modes of the entire linear chain of ions moving together as one body, with mass NM. These are called the center of mass modes. Each ω_z

quantum of vibrational energy is called a phonon, and can be thought of as a particle, just as a quantum of electromagnetic radiation in a cavity is a photon. For the above phonon description to hold, certain criteria must hold. First, the coupling to the environment must be sufficiently small such that thermalization does not randomize the state of the system (and thus cause it to behave classically). Physically, what can happen is that nearby fluctuating electric and magnetic fields push on the ions, causing their motional state to randomly transition between energy eigenstates. Such noise sources are nearly inevitable, in a technical sense, since, for example, one cannot drive the confining electrodes from a perfect voltage source; the source will always have a finite resistance, and this resistance gives rise to Johnson noise, which has fluctuations on time scales the ions are sensitive to. The electric field on local patches of the electrodes can also fluctuate, randomly driving the ions' motion. As the randomness increases, the quantum properties of the ions' state is lost, and their behavior becomes well described by classical statistical averages. For example, both their momentum and position become well defined, which cannot be simultaneously true for a quantum system. Nevertheless, in practice, most technical noise sources can indeed be controlled quite well, to the extent that they do not heat or dephase the trapped ions too much on the time scale of most experiments. In part, one important reason this is possible is that as long as the harmonic approximation holds, the trapped ions are very selective about the frequency of the noise they are sensitive to; just as transitions between atomic levels can be selected by radiation tuned only to the correct frequency, only fluctuations which have high spectral power density around ω_z will affect the ions.

It is also quite important for the ions to be sufficiently cool so as to make the one-dimensional harmonic approximation valid. The true potential is non-quadratic for large displacements along any direction away from the trap center. And higher order vibrational modes in which the ions move relative to each other (instead of moving together) must have energies much higher than the center of mass mode. When this holds, and the ions are cooled to their motional ground state, their transition to the next higher energy state is through absorption of a center of mass phonon; this process is related to the Mossba$\ddot{u}$er effect, in which a photon is absorbed by atoms in a crystal without generating local phonons because the entire crystal recoils together.

How are the ions cooled to their motional ground state? The goal is to satisfy $kBT \ll \omega_z$, where T is the temperature reflecting the kinetic energy of the ions.

Essentially, this can be done by using the fact that photons carry not only energy, but also momentum $p = h/\lambda$, where λ is the wavelength of the light. Just as the whistle of an approaching train has a higher pitch than a departing train, an atom moving toward a laser beam has transition frequencies which are slightly higher in energy than an atom moving away. If the laser is tuned such that it is absorbed only by approaching atoms, then the atoms slow down because the photons kick them in the opposite direction. This method is known as Doppler cooling. Shining a properly tuned laser (which has momentum vector components along each axis) at trapped atoms thus can cool the atoms down to the limit $kBT \approx \Gamma/2$, where Γ is the radiative width of the transition used for the cooling. To cool beyond this limit, another method, known as sideband cooling, is then applied, as illustrated in Fig2.2. This allows one to reach the $kBT \ll \omega z$ limit.

Another criterion which must be satisfied is that the width of the ion oscillation in the trap potential should be small compared to the wavelength of the incident light. This Lamb–Dicke criterion is conveniently expressed in terms of the Lamb-Dicke parameter $\eta = 2\pi z_0/\delta$, where δ is the wavelength, and $z_0 = \sqrt{\hbar/2NM\omega}$ is the characteristic length scale of the spacing between ions in the trap.

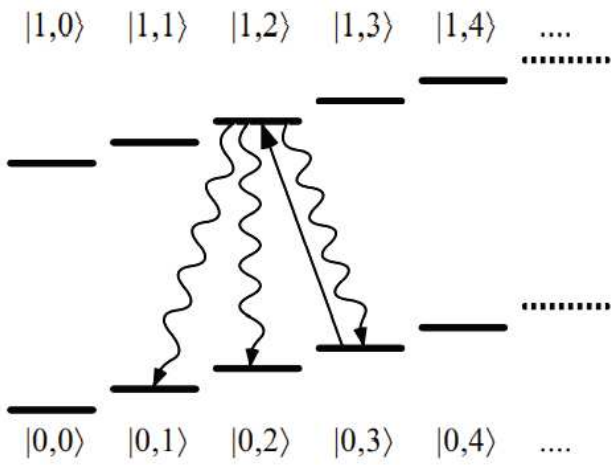

Figure 2.2: Sideband cooling method, showing transitions between $|0, n\rangle$ and $|1, m\rangle$, where 0 and 1 are two electronic levels, and n and m are phonon levels representing motional states of the ion. Laser light is tuned to have energy one phonon less than the electronic transition, such that, for example, the $|0, 3\rangle$ state transitions to the $|1, 2\rangle$ state, as shown. The atom then spontaneously decays into the lower energy 0 state (wiggly lines), randomly going to either $|0, 1\rangle$, $|0, 2\rangle$, or $|0, 3\rangle$ (with nearly equal probabilities). Note that the laser light actually causes all possible transitions between $|0, n\rangle$ and $|1, n - 1\rangle$, since these all have the same energy. However, this process does not touch the $|0, 0\rangle$ state, and eventually that is the state in which the atom will be left.

The Lamb–Dicke criterion requires that $\eta \approx 1$; this does not strictly have to be met in order for ion traps to be useful for quantum computation, but it is desired to have that $\eta \approx 1$ at least, in order that the individual ions can be resolved by different laser beams, but without making their motional state too difficult to optically excite in order to perform logic operations.

Atomic structure

The purpose of the trap apparatus described above is to allow ions to be cooled to the extent that their vibrational state is sufficiently close to having zero phonons ($|0\rangle$), an appropriate initial state for computation. Similarly, the internal states of the ions must be initialized appropriately, so they may be used to store quantum information. Let us now consider what these internal states are, and understand why they are good qubit representations by estimating their coherent lifetime.
The internal atomic states relevant to the trapped ion we shall consider result from the combination F of electron spin S and nuclear spin I, giving F = S + I. The formal piece of theory which describes this – known as the addition of angular momenta - not only describes important physics for understanding atomic structure, but also is an interesting mechanism for quantum information. A single photon interacting with an atom can provide or carry away one unit of angular momentum. But there are numerous possible sources of angular momenta in an atom: orbital, electron spin, and nuclear spin. Where it comes from is partly determined by the energy levels selected by the energy of the photon, but beyond that, the photon cannot distinguish between different sources, and to describe what happens we must select a basis in which total angular momentum becomes a uniquely defined property of the state.
Consider, for example, two spin-1/2 spins. The 'computational' basis for this two qubit space is $|00\rangle$, $|01\rangle$, $|10\rangle$, $|11\rangle$, but to span the state space we could equally well choose the basis

$$|0,0\rangle_J = \frac{|01\rangle - |10\rangle}{\sqrt{2}} \tag{2.2}$$

$$|1,-1\rangle_J = |00\rangle \tag{2.3}$$

$$|1,0\rangle_J = \frac{|01\rangle - |10\rangle}{\sqrt{2}} \tag{2.4}$$

$$|1,1\rangle_J = |11\rangle \tag{2.5}$$

$$\tag{2.6}$$

These basis states are special, because they are eigenstates of the total momentum

operator, defined by $j_x = (X_1 + X_2)/2$, $j_y = (Y_1 + Y_2)/2$, $j_z = (Z_1 + Z_2)/2$, and

$$J^2 = j_x^2 + j_y^2 + j_z^2 \tag{2.7}$$

The states $|j, m_j\rangle_J$ are eigenstates of J^2 with eigenvalue $j(j+1)$, and simultaneously eigenstates of j_z, with eigenvalue m_j . These states are the natural ones selected by many physical interactions; for example, in a $\hat{z}$ oriented magnetic field the magnetic moment μ in the Hamiltonian μB_z is proportional to m_j, the component of the total angular momentum in the $\hat{z}$ direction. The theory of addition of angular momenta is sophisticated and well developed, and we have but scratched its surface. Nevertheless, some interesting observations which concern quantum information can already be drawn from the above examples. Normally, we think of entangled states such as the Bell states as being unnatural states of matter, because they have strange, non-local properties. However, the state $|0, 0\rangle_J$ is a Bell state! Why does Nature prefer this state here? It is because of a symmetry under which the interaction involving the magnetic moment is invariant under interchange of the two spins. Such symmetries actually occur widely in Nature, and are potentially quite useful for performing entangling measurements and operations.

How long can a superposition of different spin states exist? The limiting process, known as spontaneous emission, occurs when an atom transitions from its excited state to its ground state by emitting a photon. This happens at some random time, at a rate which we shall estimate. It might seem that spontaneously emitting a photon is a strange thing for an atom to do, if it is simply sitting in free space with nothing apparently disturbing it. But this process is actually a very natural consequence of the coupling of the atom to electromagnetic fields, described simply by the Jaynes–Cummings interaction

$$H_I = g(a^\dagger \sigma_- + a\sigma_+), \tag{2.8}$$

Previously, we used this model to describe how a laser interacts with an atom, but the model also describes what happens to an atom even when no optical field is present! Consider an atom in its excited state coupled to a single mode which contains no photon, the state $|01\rangle$ (using $|field, atom\rangle$). This is not an eigenstate of H_I , and thus it cannot remain stationary as time evolves. What happens is described by the unitary operator U, by which we find that there is a probability $p_{decay} = |\langle 10|U|01\rangle|^2$ for the atom to decay into its ground state and

emit a photon, where

$$p_{decay} = g^2 \frac{4 \sin \frac{1}{2}(\omega - \omega_0)^2 t^2}{(\omega - \omega_0)^2} \tag{2.9}$$

to lowest order in g, the atom–field coupling, ω is the frequency of the photon, and $\hbar\omega_0$ the energy difference between the two levels of the atom. An atom sitting in free space interacts with many different optical modes; inserting the coupling

$$g^2 = \frac{\omega_0^2}{2\hbar\omega\epsilon_0 c^2} |\langle 0|\vec{\mu}|1\rangle|^2 \tag{2.10}$$

here $\vec{\mu}$ is the atomic dipole operator, integrating over all the optical modes and taking a time derivative gives the probability per second of decay,

$$\gamma_{rad} = \frac{\omega_0^3 |\langle 0|\vec{\mu}|1\rangle|^2}{3\pi\hbar\epsilon_0 c^5} \tag{2.11}$$

If we make the approximation that $|\langle 0|\vec{\mu}|1\rangle| \approx \mu B \approx 910^{-24} J/T$, the Bohr magneton, and assume that $\omega_0/2\pi \approx 10GHz$, then $y_{rad} \approx 10^{-15} sec^{-1}$, a spontaneous emission rate of less than one decay every 3 000 000 years. This calculation is representative of those done to estimate lifetimes of atomic states; as you can see, the hyperfine states can have remarkably long coherence times in theory, and this is generally consistent with experiments, in which lifetimes of tens of seconds to tens of hours have been observed.

2.2 The Hamiltonian

Combining the simplified models given in the previous section for the harmonic electromagnetic trap and the atomic structure provides us with the following simplified toy model for an ion trap quantum information processor. Imagine a single two-level spin interacting via the usual magnetic dipole interaction $H_I = -\vec{\mu} \cdot \vec{B}$ with an electromagnetic field, where the dipole moment $\vec{\mu} = \mu_m \vec{S}$ is proportional to the spin operator S, and the magnetic field is $\vec{B} = B_1 \hat{x} \cos(kz - \omega t + \phi)$, and B_1 is the field strength, k its momentum in the $\hat{z}$ direction, ω its frequency, and ϕ its phase. Note that in this section, we shall use $S_x = X/2$, $S_y = Y/2$, and $S_z = Z/2$ as the spin operators; they are related to the Pauli operators by a factor of two. In addition to the usual electromagnetic interaction, there are interactions with the vibrational modes. The spin is physically confined within a harmonic poten-

tial of energy scale $\hbar\omega_z$ (Fig. 2.3), such that its position becomes quantized and we must describe it by an operator $z = z_0(a^\dagger + a)$, where $a^\dagger$, a are raising and lowering operators for the vibrational modes of the particle, representing creation and annihilation of phonons.

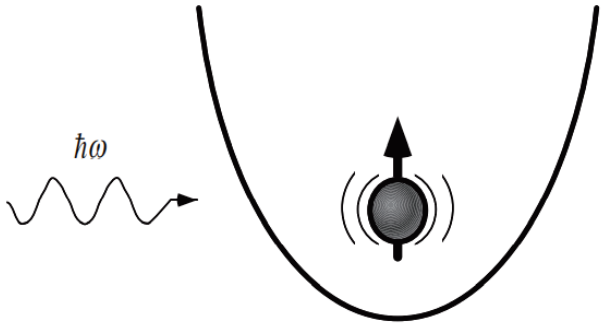

Figure 2.3: Toy model of a trapped ion: a single particle in a harmonic potential with two internal states, interacting with electromagnetic radiation.

Let us assume that the particle is cooled to near its lowest vibrational mode, such that the width of its oscillation in the well is small compared to the wavelength of the incident light, that is, the Lamb–Dicke parameter $\eta \equiv kz_0$ is small. Defining the Rabi frequency of the spin as $\omega = \mu_m B_1/2$, and recalling that $S_x = (S_+ + S_-)/2$, we find that the interaction Hamiltonian simplifies in the small η limit to become

$$H_I = -\vec{\mu} \cdot \vec{B} \tag{2.12}$$

$$\approx [\frac{\hbar\Omega}{2}(S_+ \mathrm{e}^{i(\phi-\omega t)} + S_- \mathrm{e}^{-i(\phi-\omega t)})] \tag{2.13}$$

$$+ [i\frac{\eta\hbar\Omega}{2}\{S_+ a + S_- a^\dagger + S_+ a^\dagger + S_a\}(\mathrm{e}^{i(\phi-\omega t)} + \mathrm{e}^{-i(\phi-\omega t)})] \tag{2.14}$$

The first term in brackets results from the usual Jaynes–Cummings Hamiltonian which occurs when the location z of the spin is a constant. However, it is simplified and does not contain photon operators because it turns out that as long as B_1 is a strong coherent state, we can neglect its quantum properties and leave ourselves with a Hamiltonian which describes just the evolution of the internal atomic state. It is in fact quite remarkable that a coherent state of the field does not become entangled with an atom after interacting with it. The second term in brackets describes the coupling of the motional state of the ion to its spin state, through the fact that the magnetic field it sees is dependent on its position. The

four terms in braces correspond to four transitions (two up and two down) which are known as the red and blue motional sidebands, illustrated in Fig. 2.4.

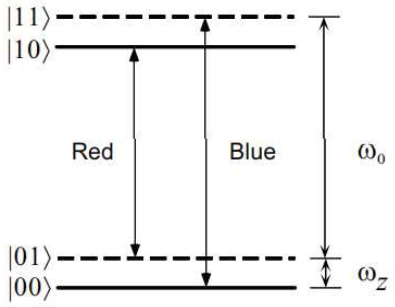

Figure 2.4: Energy levels of the toy model trapped ion showing the red and blue motional sideband transitions, which correspond to creation or annihilation of a single phonon. There is an infinite ladder of additional motional states, which are usually not involved. The states are labeled as $|n, m|$ where n represents the spin state, and m the number of phonons.

Why these sideband transitions have frequencies $\omega_0 \pm \omega_z$ is easy to see, by including the free particle Hamiltonian

$$H_0 = \hbar\omega_0 S_z + \hbar\omega_z a^\dagger a \tag{2.15}$$

which causes the spin and phonon operators to evolve as

$$\begin{aligned} S_+(t) &= S_+ \mathrm{e}^{i\omega_0 t} & \qquad S_-(t) &= S_- \mathrm{e}^{-i\omega_0 t} \\ a^\dagger(t) &= a^\dagger \mathrm{e}^{i\omega_z t} & \qquad a(t) &= a\mathrm{e}^{-i\omega_z t}. \end{aligned} \tag{2.16}$$

Thus, in the frame of reference of H_0, the dominant terms of $H_I^{'} = \mathrm{e}^{iH_0 t/\hbar} H_I \mathrm{e}^{-iH_0 t/\hbar}$ are found to be

$$H_I^{'} = \begin{cases} i\frac{\eta\hbar\Omega}{2}(S_+ a^\dagger \mathrm{e}^{i\varphi} - S_- a\mathrm{e}^{-i\varphi}) & \omega = \omega_0 + \omega_z \\ i\frac{\eta\hbar\Omega}{2}(S_+ a\mathrm{e}^{i\varphi} - S_- a^\dagger \mathrm{e}^{-i\varphi}) & \omega = \omega_0 - \omega_z \end{cases} \tag{2.17}$$

where the frequency of the electromagnetic field, ω, is as shown on the right. Extending the above model from one spin to N spins confined within the same harmonic potential is simple if we assume that they share a single center of mass vibrational mode, whose energy is much lower than any other vibrational mode of the system. A straightforward extension of the theory shows that the only required modification is replacement of Ω by $\Omega/\sqrt{N}$, since all N particles move together collectively.

2.3 Quantum Computation

Quantum computation with trapped ions requires one to be able to construct arbitrary unitary transforms on the internal states of the atoms. We now show how this is done, in three steps: we describe (1) how arbitrary single qubit operations are performed on the internal atomic (spin) state, (2) a method for performing a controlled two qubit gate between the spin and the phonon state, and (3) a way to swap quantum information between the spin and the phonon. Given these building blocks, we then describe an experiment which was performed to demonstrate a controlled- gate, complete with state preparation and readout.

Single qubit operations

Applying an electromagnetic field tuned to frequency ω_0 turns on the internal Hamiltonian term

$$H_I^{internal} = \frac{\hbar\Omega}{2}(S_+ \mathrm{e}^{i\varphi} + S_- \mathrm{e}^{-i\varphi}) \tag{2.18}$$

By choosing ϕ and the duration of the interaction appropriately, this allows us to perform rotation operations $R_x(\theta) = exp(-i\theta S_x)$ and $R_y(\theta) = exp(-i\theta S_y)$, which, by the Theorem of Z-Y decomposition for a single qubit, thereby allow us to perform any single qubit operation on the spin state. We shall denote rotations on the jth ion by a subscript, for example, $R_{xj}(\theta)$.

Controlled phase-flip gate

Suppose, now, that one qubit is stored in the atom's internal spin state, and another qubit is stored using the $|0\rangle$ and $|1\rangle$ phonon states. If this is the case, we can perform a controlled phase-flip gate, with the unitary transform

$$\begin{bmatrix} 1 & 0 & 0 & 0 \\ 0 & 1 & 0 & 0 \\ 0 & 0 & 1 & 0 \\ 0 & 0 & 0 & -1 \end{bmatrix} \tag{2.19}$$

It is easiest to explain how to do this with an atom that has a third energy level, as shown in Figure 7.11 (the extra level is not fundamentally necessary; see Problem 7.4). A laser is tuned to the frequency $\omega_{aux} + \omega_z$, to cause transitions between the $|20\rangle$ and $|11\rangle$ states; this turns on a Hamiltonian of the form

$$H_{aux} = i\frac{\eta\hbar\Omega'}{2}(S'_+ \mathrm{e}^{i\varphi} + S'_- \mathrm{e}^{-i\varphi}) \tag{2.20}$$

where S'_+ and S'_- denote transitions between $|20\rangle$ and $|11\rangle$, and we assume that higher order motional states are unoccupied. Note that because of the uniqueness of this frequency, no other transitions are excited. We apply the laser with phase and duration to perform a 2π pulse, that is, the rotation $R_x(2\pi)$ on the space spanned by $|11\rangle$ and $|20\rangle$, which is just the unitary transform $|11\rangle \rightarrow -|11\rangle$. All the other states remain unchanged, assuming that undesired states such as $|1,2\rangle$ have no probability amplitude. We shall write this gate as $C_j(Z)$ (denoting a controlled-Z operation), where j indicates which ion the gate is applied to. Note that the same phonon is shared by all the ions, since it is a center-of-mass phonon; because of this, adopting engineering terminology, this has been called the phonon 'bus' qubit in the literature.

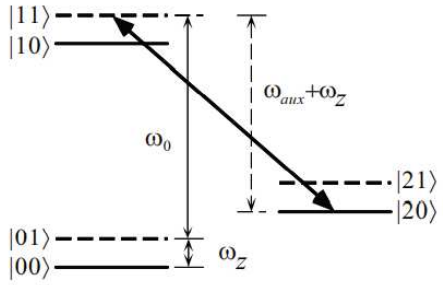

Figure 2.5: Energy levels of a three-level atom in an ion trap, with two phonon states each. The labels $|n,m\rangle$ indicate the atom's state n and the phonon state m. The $|20\rangle \rightarrow |11\rangle$ transition is used to perform a controlled phase-flip gate.

Swap gate

Finally, we need some way to swap qubits between the atom's internal spin state and the phonon state. This can be done by tuning a laser to the frequency $\omega_0 - \omega_z$, and arranging for the phase to be such that we perform the rotation $R_y(\pi)$ on the subspace spanned by $|01\rangle$ and $|10\rangle$, which is just the unitary transform

$$\begin{bmatrix} 1 & 0 & 0 & 0 \\ 0 & 0 & 1 & 0 \\ 0 & -1 & 0 & 0 \\ 0 & 0 & 0 & 1 \end{bmatrix} \tag{2.21}$$

on the $|00\rangle$, $|01\rangle$, $|10\rangle$, $|11\rangle$ space. If the initial state is $a|00\rangle + b|10\rangle$ (that is, the phonon is initially $|0\rangle$), then the state after the swap is $a|00\rangle + b|01\rangle$, so this

accomplishes the desired swap operation. We shall write this as j when acting on ion j; the inverse operation $\overline{SWAP}_j$ corresponds to $R_y(-\pi)$. Technically, because of the minus sign in the $|10\rangle\langle 01|$ entry of $R_y(\pi)$, this is not a perfect swap operation, but it is equivalent to one up relative phases. Thus, this is sometimes referred to as being a 'mapping operation' instead of a swap.

Controlled-NOT gate

Putting these gates together allows us to construct a gate acting on ions j (control) and k (target) using the sequence of operations

$$CNOT_{jk} = H_k \; \overline{SWAP}_k \; C_j(Z) \; SWAP_k \; H_k \tag{2.22}$$

(time going from right to left, as usual for matrices) where H_k is a Hadamard gate (constructed from R_y and R_x rotations on ion k).

2.4 Experiment

A controlled-NOT gate using a single trapped ion has been demonstrated [5]. In the experiment, a single ion of $^9Be^+$ is trapped in a coaxial resonator RF ion trap, different in geometry from the linear ion trap of Fig2.1. Beryllium was chosen for its convenient hyperfine and electronic level structure, shown in Fig2.6. The $^2S_{1/2}(1,1)$ and $^2S_{1/2}(2,2)$ energy levels are used as the atom's internal qubit state, and the $|0\rangle$ and $|1\rangle$ phonon states as another qubit
in the figure as $n = 0$ and $n = 1$). The $\approx 313nm$ transition between the $^2S_{1/2}(1,1)$ and $^2S_{1/2}(2,2)$ levels is accomplished not by tuning a single laser to the transition frequency, but rather two lasers whose difference frequency is that of the transition. This Raman transition method simplifies requirements for laser phase stability. The $^2S_{1/2}(2,0)$ state is used as the auxiliary level; the $2S1/2$ states have different energies by virtue of a 0.18 millitesla magnetic field applied to the system. The trapped ion has vibrational frequencies $(\omega_x, \omega_y, \omega_z)/2\pi = (11.2, 18.2, 29.8)MHz$ in the trap, and a ground state $n_x = 0$ wavefunction spread of about $7nm$, giving a Lamb–Dicke parameter of about $\eta_x = 0.2$. The Rabi frequency of the on-resonance transition is $\Omega/2\pi = 140kHz$, the two motional sidebands, $\eta_x\Omega/2\pi = 30kHz$, and the auxiliary transition $\eta_x\Omega'/2\pi = 12kHz$. The state of the ion is initialized using Doppler and sideband cooling to obtain, with approximately 95% probability, the state $|00\rangle = |^2S_{1/2}(2,2)\rangle|n_x = 0\rangle$. The internal and

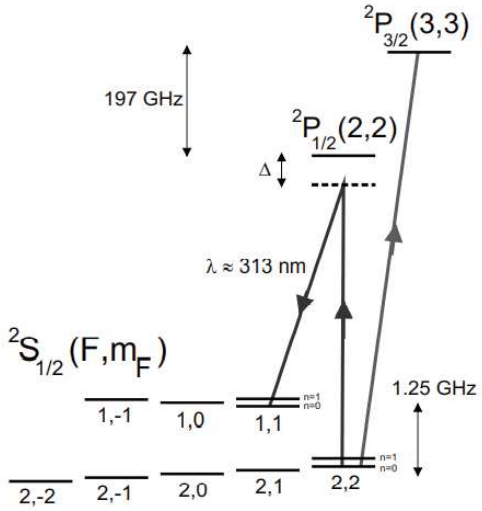

Figure 2.6: Energy levels of $^9Be^+$ used in the ion trap experiment.

motional states of the ion are then prepared in one of the four basis states $|00\rangle$, $|01\rangle$, $|10\rangle$, or $|11\rangle$ using single qubit operations, then a controlled- gate is performed using three pulses, which implement a $R_y(\pi/2)$ rotation on the internal state qubit, a controlled-Z operation between the two qubits, then a $R_y(-\pi/2)$ rotation on the internal state qubit. It is simple to show (Exercise 7.32) that this circuit, drawn in Figure 7.14, realizes a controlled- gate. Readout of the computational output is performed with two measurements. The first is to collect the fluorescence from the ion which occurs when + circularly polarized light tuned to the $^2S_{1/2}(2,2)$–$^2P_{3/2}(3,3)$ 'cycling' transition is applied. The light does not couple appreciably to the $^2S_{1/2}(1,1)$ state, and thus the intensity of the observed fluorescence is proportional to the probability of the internal state qubit being in the $|0\rangle$ state; it is a projective measurement. This measurement technique is powerful because the transition cycles many times - the ion absorbs a photon, jumping to the $^2P_{3/2}(3,3)$ state, then emits a photon, decaying back into the $^2S_{1/2}(2,2)$ state where it started. Thousands or more cycles are possible, allowing good statistics to be accumulated. The second measurement is similar to the first, but a swap pulse is applied first to exchange the motional and internal state qubits; this projectively measures the motional state qubit The experiment as performed verifies the classical truth table of the controlled operation and, in principle, by preparing superposition input states and measuring output density matrices, the unitary transform could be completely characterized using process tomography (Chapter 8). The controlled-gate requires about 50 microseconds to perform with the optical power used in the experiment. On the other hand, the

coherence time was measured to be somewhere around hundreds to thousands of microseconds. The dominant decoherence mechanisms included instabilities in the laser beam power and the RF ion trap drive frequency and voltage amplitude, and fluctuating external magnetic fields. Moreover, the experiment involved only a single ion, and only two qubits, and thus was not useful for computation; to be useful, a controlled- gate should generally be applied between different ions, and not just between a single ion and the motional state. However, the technical limitations can probably be overcome, and lifetimes can be extended by using the short-lived motional state only intermittently, capitalizing on the much longer coherence times of the internal atomic states. And scaling to larger numbers of ions is conceptually viable. Shown in Figure 7.15 is a string of 40 mercury ions which have been trapped. There are many hurdles to making such systems behave as useful quantum information processing machines, but technological surprises are a neverending saga. Someday, perhaps, trapped ions such as these could be registers of qubits in a quantum computer.

Figure 2.7: Image of fluorescence from about 40 trapped mercury ($^{199}Hg^{+}$) atomic ions. The ions are spaced by approximately 15 micrometers, and the two apparent gaps are different isotopes of mercury which do not respond to the probe laser. Reprinted courtesy of D. Wineland, at NIST.

2.5 Ion Trap Quantum Computer

- Qubit representation: Hyperfine (nuclear spin) state of an atom, and lowest level vibrational modes (phonons) of trapped atoms.

- Unitary evolution: Arbitrary transforms are constructed from application of laser pulses which externally manipulate the atomic state, via the Jaynes–Cummings interaction. Qubits interact via a shared phonon state.

- Initial state preparation: Cool the atoms (by trapping and using optical pumping) into their motional ground state, and hyperfine ground state.

- Readout: Measure population of hyperfine states.
- Drawbacks: Phonon lifetimes are short, and ions are difficult to prepare in their motional ground states

Chapter 3

Superconducting Quantum Computer

3.1 Superconducting qubits

These qubits are created by reducing the temperature of a material to make it become a better conductor, in some materials the resistance drops to near 0 after reaching a really low temperature, such materials are known as superconductors. With the proper conditions electronic circuits made with these superconductors show quantum properties which allows them to be used for quantum computing. To maintain these low temperatures, a dilution refrigerator is needed. Furthermore, to interact with the qubits, microwave equipment is used. The combination of these two devices allows to operate the qubits and keep them cold. The main benefit of this type of qubit is that it comes on a chip, just like classical CPUs. Additionally, superconducting qubits are compatible with existing fabrication infrastructure and have high fidelity gates and readout. However, these qubits do have their drawbacks, including the need to cool the material at microkelvin, which will require bigger dilution fridges with more qubits.

The advantage of quantum superconducting circuits (QSC) as implementation of qubits is, first and foremost, due to the macroscopically quantum coherent ground state of super-conductors, which (a) supports non-dissipative flow of electrical current and (b) suppresses or outright eliminates low-energy elementary excitations. The latter property counterweighs the dangerous effects of a huge number degrees of freedom, which exist in the solid state and which would otherwise severely limit or totally destroy the quantum coherence necessary for the operation of a quantum computer In this way the primary advantage of QSC

allows the realization of the secondary one: as a solid state based device, a superconducting qubit and a more complex QSC can be more easily scaled up, can have significant density, and can be produced using a well developed set of design and fabrication methods. Moreover, since these circuits are macroscopic, it can be simpler to manipulate and read their state. The necessity to operate at low temperatures is not a disadvantage of QSC, since almost all the quantum information processing requires low temperatures in order to suppress the effects of noise.

DiVincenzo criteria

According to DiVincenzo's criteria, constructing a quantum computer capable of quantum computation requires that the experimental setup meet five conditions:

- A scalable physical system with well-characterized qubit
- The ability to initialize the state of the qubits to a simple fiducial state
- Long relevant decoherence times
- A "universal" set of quantum gates
- A qubit-specific measurement capability

The DiVincenzo criteria reflect the contradictory requirements to a quantum computer implementing the quantum circuits approach: on the one hand, the qubits must be maximally protected from the external influences to preserve quantum coherence; on the other hand, the need to do precise time-domain manipulations on them leads to complex control-and-readout circuitry, which will introduce decoherence into the system. The major success of quantum information theory has been to show that quantum error correction is possible and that therefore the computation time is not limited by the coherence time. As long as the error probability per gate is below a certain threshold, one is able to do arbitrary long quantum computations.

Josephson effect

We have seen that a qubit must have two well defined levels that are used as logical states $|0\rangle$ and $|1\rangle$. However, in practice, very few systems in nature are defined by only two levels. To get around this, we can take two states in a nonlinear system and treat them as an effective localized $\text{spin}_{1/2}$ (qubit). Due to

nonlinearity, the transitions to other states can be made practically negligible. In electrical circuits, the natural solution is a superconducting Josephson junction: the only known nonlinear and nondissipative electrical element.

Josephson junctions

Josephson junctions are formed by two superconductors separated by a weak link. "Weak" means that the probability amplitude for an electron to pass through the link must be small enough to be considered as a perturbation. The coherent nondissipative current is carried by the Bose-condensate of Cooper pairs of electrons with (in most superconductors) opposite spins. A bulk superconductor is characterized by a position-dependent complex superconducting order parameter Δ which up to a factor can be written as $\sqrt{n_s}\ exp(i\phi)$, where n_s is the average density of electrons in the condensate, and ϕ is related to the velocity of supercurrent. The supercurrent density is given by $\vec{j_s} = n_s e\vec{v_s}$. Following the approach due to Feynman we neglect the variation of the order parameter within each superconductor and describe the system by a two-component "wave function", $\Psi = (\sqrt{n_{s,1}}\ exp(i\phi_1), \sqrt{n_{s,2}}\ exp(i\phi_2))^T$. Now, assume that there is a voltage diffence V between the superconductors, which means that the energy difference between them is $2eV$ (since the Cooper pair has charge $2e$). Then the Schrödinger equation for Ψ can be written as

Figure 3.1: The electrical symbol for a Josephson junction

$$i\hbar\frac{\partial}{\partial t}\begin{pmatrix}\sqrt{n_{s,1}}\mathrm{e}^{i\phi_1}\\ \sqrt{n_{s,1}}\mathrm{e}^{i\phi_1}\end{pmatrix} = \begin{pmatrix}eV & K\\ K & -eV\end{pmatrix}\begin{pmatrix}\sqrt{n_{s,1}}\mathrm{e}^{i\phi_1}\\ \sqrt{n_{s,1}}\mathrm{e}^{i\phi_1}\end{pmatrix} \tag{3.1}$$

After a simple calculation we find that $dn_{s,1}/dt = (2Kn_{s,1}/\hbar)sin(\phi_2 - \phi_1)$; $d(\phi_2 - \phi_1)/dt = 2eV/\hbar$ that is, the celebrated formulae for the DC and AC Josephson effect:

$$I_J = I_c \sin\phi; \qquad \dot{\phi} = 2eV/\hbar. \tag{3.2}$$

The first equation in (3.2) describes the non-dissipative, equilibrium, coherent flow of electric current through the barrier, determined only by the phase difference between the superconductors and the properties of the junction. The second equation (3.2) tells that if the phase difference is not constant, the current flow will be accompanied by a finite voltage drop across the junction, and vice versa. The equilibrium current can be obtained from the appropriate thermodynamical potential of the system: $I_J = \partial E/\partial\Phi$, where $\Phi = \Phi_0\phi/2\pi$ has the dimensional-

ity of the magnetic flux, and $\Phi_0 = h/2e$ is the superconducting flux quantum. Therefore we add to the energy of the system its Josephson energy,

$$E_J(\phi) = \int d\Phi I_J(\phi) = -\frac{I_c \Phi_0}{2\pi} \cos\phi \equiv -E_J \cos\phi. \tag{3.3}$$

From the AC Josephson effect and according to the relation $V = L\dot{I}$, we see that the Josephson junction can be considered as a nonlinear inductance L_J :

$$L_J = \frac{\hbar}{2eI_c \cos\phi} \tag{3.4}$$

As an example of this quantum inductance, consider the rf-SQUID: a superconducting loop of inductance L interrupted by a single Josephson junction.

In this configuration the total energy of a Josephson junction also includes its electrostatic energy:

$$E = Q^2/2C + E_J(\phi) = E_c(N_c - N_g)^2 + E_J(\phi) \tag{3.5}$$

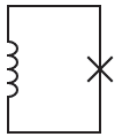

Figure 3.2: Schema elettrico di un rf-SQUID

Here Q is the electric charge on the junction's capacitance, C, and $E_C = 4e^2/2C$ the charging energy (the Coulomb energy of one Cooper pair). The charge Q is expressed through N_C and N_g. The former is the number of Cooper pairs having tunneled through the junction while the latter depends on the system's configuration and its electrostatic interaction with its surroundings. While N_C is a discrete number, N_g can take arbitrary values. To certain extent, N_C and ϕ can be considered as conjugate variables, like momentum and position, therefore we can quantize Eq.3.5:

$$H = E_C(-i\partial_\phi - N_g)^2 - E_J \cos\phi. \tag{3.6}$$

Taking $N_g = 0$ and expanding the cosine around $\phi = 0$, we obtain the Hamiltonian of a linear oscillator with the eigenfrequency ω_0 : $-\omega_0^2\phi = (i\hbar)^{-2}$, that is $\hbar\omega_0 = \sqrt{2E_C E_J}$. In practice, this plasma frequency is in the range of tens of GHz.

3.2 Types of Superconductive Qubits

Three main classes of superconducting qubits, all based on Josephson junctions, have been theoretically studied and tested experimentally. These are phase, flux and charge qubits. The relation between the parameters $\hbar\omega_0$, E_C and E_J and the

way these qubits are biased distinguishes between the different types.

The Phase Qubit

Phase qubits operate in the phase regime, which is defined by $E_J \gg E_C$. In this situation, the Josephson term dominates the Hamiltonian (3.6)

$$H = -E_c\partial_\phi^2 - E_J\cos\phi - \frac{I_b\Phi_0}{2\pi}\phi \equiv -E_c\partial_\phi^2 - E_J(\cos\phi + \frac{I_b}{I_c}\phi), \tag{3.7}$$

where the last term describes the effect of the external bias current I_b. This is the Hamiltonian of a quantum particle in a tilted *washboard potential*. Since $E_J \gg E_C$, in the absence of bias ($I_b = 0$), each energy well contains many almost equidistant quantized levels and the tunneling bethween different minima is negligible. On the other hand, the Josephson junction cannot support a nondissipative current exceeding I_c, in which case te potential in (3.7) no longer has local minima. In the subcritical regime, when I_b is between $0.95I_c$ and $0.98I_c$, there remain only a few quantized level in every local minumum. The tunneling out of the first two levels in a given potential through the barrier is still small enough, and these can be taken as qubit states $|0\rangle$ and $|1\rangle$. When $I_b \approx I_c$ the phase $\phi \approx \pi/2$; expanding the Josephson potential in (3.7) to the third order in $\varphi \equiv \phi - \pi/2$, we find

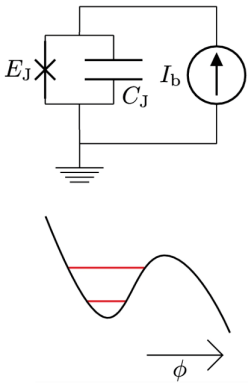

Figure 3.3: Basic Josephson-junction Phase qubit circuit and its potential-energy chart, with the two lowest energy levels marked in red.

$$U_J(\varphi) = E_J[(1 - I_c/I_b)\varphi - \varphi^3/6] \tag{3.8}$$

The plasma frequency of the resulting cubic oscillator is $\omega_p(I_b) = \omega_0(1 - (I_b/I_c)^2)^{1/4}$. The transition frequency between the two qubit states is $\omega_{01} \approx 0.95\omega_p$ and depends on the bias current. Now the Hamiltonian (3.7) can be written simply as $H = -\frac{\hbar\omega_{01}}{2}\sigma^2$, corresponding to a spin-1/2 in a field along the z direction. The x- and y- components, necessary for unitary rotations of the qubit, can be implemented by adding an oscillating component to the bias current at the qubit transition frequency ω_{01}: $I_b = I_{b,dc} + I^c_{b,ac}\cos\omega_{01}t + I^s_{b,ac}\sin\omega_{01}t$. The effective Hamiltonian becomes

$$H = -\frac{\hbar\omega_{01}}{2}\sigma^Z + \sqrt{\frac{\hbar}{2\omega_{01}C}}\frac{I^s_{b,ac}}{2}\sigma^x + \sqrt{\frac{\hbar}{2\omega_{01}C}}\frac{I^c_{b,ac}}{2}\sigma^y. \tag{3.9}$$

The DC component of the bias current sets $\omega 01$, while the cosine and sine quadratures produce the rotations around the x and the y axis, respectively. The nonlinearity of the potential (3.8) is crucial, otherwise the AC current pulses would also excite transitions between higher levels, and out of the Hilbert space spanned by $|0\rangle$ and $|1\rangle$. In other words, the system would no longer be a qubit. Advantages of phase qubits include the simplicity of design, good control over the parameters in the Hamiltonian, simple readout, weak sensitivity to charge and flux noise in the system, and scalability. One of the disadvantages is the sensitivity to low-frequency noise of critical and bias current. Another is the absence of the optimal point (degeneracy point where symmetry would protect the qubit from certain kinds of noise leading to an increese in coherance times). One other disadvantage would be requiring complex high-frequency low-noise circuitry down to the very low operating temperatures ($\sim 10mK$). On the other hand, using AC rather than DC pulses allows for protection by low-pass filtration of the qubit from the low frequency ($1/f$) noise coming from the bias lines that can be significant.

The Flux Qubit

Another possibility to realize a qubit in the phase limit $E_J \gg E_C$ is by using a degeneracy between two current-carrying states of an RF-SQUID. In writing the Hamiltonian of the system, the only difference with respect to the Hamiltonian of Eq.(3.6) is that we now must take into account of the magnetic energy, but can neglect the effect of off-set charges N_g:

$$H = -E_C \partial_\phi^2 - E_J \cos\phi + E_L(\phi - \phi_x)^2/2 \qquad (3.10)$$

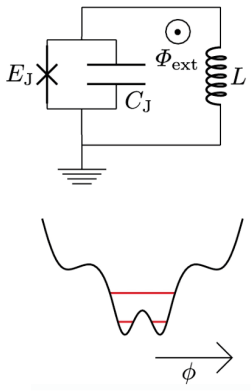

Figure 3.4: Basic Josephson-junction Flux qubit circuit and its potential-energy chart, with the two lowest energy levels marked in red.

Here $\phi_x = 2\pi\Phi/\Phi_0$ is the reduced flux through the loop, and the inductive energy scale is given by $E_L = \Phi_0^2/4\pi L$. The situation differs from the previous case because now, if $\phi_x \approx \pi$, the potential energy formed by the last two terms of (3.10) has two almost degenerate minima. These states correspond to persistent current in the loop circulating in opposite directions, and are conveniently used as the $|0\rangle$ and $|1\rangle$ states of a qubit. Tunneling between the two potential wells is enabled by the charge term in (3.10). As a result, in

the subspace $|0\rangle$, $|1\rangle$ the effective qubit Hamiltonian is

$$H = -\frac{\epsilon}{2}\sigma^z + \frac{\Delta}{2}\sigma^x, \tag{3.11}$$

where ϵ is the energy bias between the two states, which is tuned by the external flux; δ is the tunneling amplitude. When $\epsilon \gg \Delta$, the eigenstates of (3.12) coincide with $|0\rangle$ and $|1\rangle$. At the degeneracy point, $\epsilon = 0(\phi_x = \pi)$, these erigenstates are "bonding/antibonding" states $|\pm\rangle = (|0\rangle \pm |1\rangle)/\sqrt{2}$. The expectation value of the current circulating in the SQUID loop is the same. As a result, the states cannot be distinguished by observing the current or the magnetic field it produces. Therefore no external degrees of freedom that couple to magnetic field can interface with the qubit when it is operated at this optimal point; e coherence time of the qubit can thus be significantly enhanced. Therefore it is convenient to always work at this special operating point and use the corresponding eigenstates as effective logical states of the qubit: $|0_L\rangle = |+\rangle, |1_L\rangle = |-\rangle$. While the Hamiltonian (3.12) enables all qubit rotations with DC pulses only, transitions between these states can also be realized by applying RF flux pulses at the transition frequency, same as in a phase qubit. Advantages of flux qubits are their weak sensitivity to charge noise, comparatively easy readout, the ability to work at or near the degeneracy point (optimal point). Their main disadvantage is a very strong dependence on the junction parameters. The tunneling splitting Δ is proportional to $\sqrt{E_J E_C}\mathrm{e}^{[-\sqrt{E_J/E_C}]}$, while E_J itself depends exponentially on the barrier thickness. Such fluctuations as $1/f$ noise in the critical current will thus have a big effect on the qubit.

The Charge Qubit

The charge qubit operates in the opposite regime from the previous two types of qubits, the charge limit $E_C \gg E_J$. Now the states with definite charge, differing by a single Cooper pair, are the working states of the qubit, and the Josephson term is the perturbation. In order for a single Cooper pair to make a difference, two conditions must be met. The charging energy $E_C \sim e^2/C$ must far exceed both the thermal energy, $k_B T$, and the linewidth of the charge states, $\Delta E \sim \hbar/RC$, due to their finite lifetime determined by the effective resistance and capacitance of the system. Otherwise, the charge states are smeared out and cannot form a good basis for a qubit. The second condition leads to the requirement $R > \hbar/e^2 \sim 6k\Omega$. This becomes a problem, because at GHz frequencies dictated by small capacitances C, the tunneling resistance will be effectively

shunted by small impedance $\sim 50 - 100\Omega$ of the connecting lead. This way the charge states would be washed out by the quantum particle number fluctuations.

The Hamiltonian for a charge qubit can be written as the sum of the electrostatic energy and of the Josephson energy:

$$H = E_C(N_C - N_g)^2 - E_J \cos\phi \tag{3.12}$$

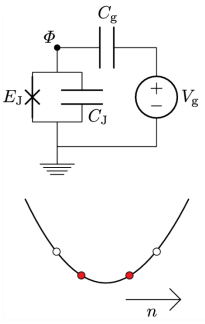

Figure 3.5: Basic Josephson-junction Charge qubit circuit and its potential-energy chart, with the two lowest energy levels marked in red.

In the absence of Josephson energy, the states $|N_C = 0\rangle$ and $|N_C = 1\rangle$ are degenerate when $N_g = C_g V_g/2e = 1/2$. Higher-energy states can be neglected; then on the Hilbert subspace spanned by these two states, the operator N_C takes the form $N_C = \frac{1}{2}(1 - \sigma z)$. The Josephson term lifts the charge degeneracy; in this basis it can be written as $E_J\sigma^x/2$. The Hamiltonian again takes the pseudospin form

$$H = -\frac{1}{2}E_C(1 - 2N_g)\sigma^z - \frac{E_J}{2}\sigma^x, \tag{3.13}$$

allowing all unitary rotations with DC pulses only. t the charge degeneracy point, $N_g = 1/2$, the eigenstates of this Hamiltonian are coherent superpositions of states $(|0\rangle \pm |1\rangle)/\sqrt{2}$ differing by a single Cooper pair. Like in the flux case, it is best to operate at this optimal point, and it is convenient to make a transformation to the basis of logical qubit states $(|0\rangle \pm |1\rangle)/\sqrt{2} : \sigma^x \leftarrow -\sigma^z and \sigma^z \leftarrow \sigma^x$. Then denoting $N_g = 1/2 + N_{g,ac}\cos(\omega t)$, we have

$$H = \frac{E_J}{2}\sigma^z + E_C N_{g,ac}\cos(\omega t)\sigma^x. \tag{3.14}$$

Now the Josephson energy plays the role of transition frequency for the qubit and AC voltage $N_{g,ac}$ can be used to induce transitions between these states. The advantages of the charge qubit operating at the optimal point are similar to those of the flux qubit. The former however does not have the exponential dependance on parameters that the flux qubit has. One of its main disadvantages is very strong sensitivity to charge noise. This can be mitigated to some extent by working in the intermediate regime, $E_J \lesssim E_C$, which was realized in the "transmon" qubit.

3.3 Further Josephson-Junction Qubits

The Transmon Qubit

The transmon qubit [7] is formed by adding another capacitance C_B, in parallel with the Josephson junction, to the charge-qubit circuit in Fig.3.5. Adding the extra capacitance decreases the charging energy E_C in the circuit. By changing the E_J/E_C ratio from $E_J/E_C \approx 10^{-1}$ to $E_J/E_C \approx 10^2$, the charge-qubit circuit goes from having a well-defined n to having a well-defined ϕ. However, the resulting energy levels are largely insensitive to fluctuations in n_g, as shown in Fig.

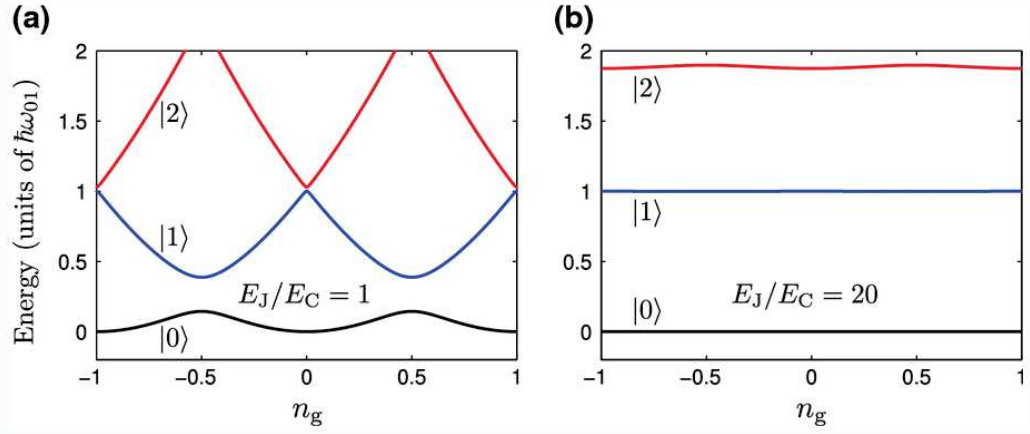

Figure 3.6: Energy levels of a CPB for different EJ/EC ratios. **a** This is the charge-qubit regime, where a good qubit is formed when $n_g \approx \pm 0.5$. At these points, ω_{01} is nowhere close to ω_{12} and the transition frequencies are not so sensitive to fluctuations in n_g. **b** $E_J/E_C = 20$. This is the transmon-qubit regime, where the energy levels are insensitive to fluctuations in n_g no matter what the value of n_g is.

The price one pays for this protection from charge noise is a decrease in the anharmonicity of the circuit. In the limit $E_J \gg E_C$, perturbation theory in the small variable E_C/E_Jgives that the energy levels Em of the circuit are well approximated by

$$E_m = -E_J + \sqrt{8E_J E_C}(m + \frac{1}{2}) - \frac{E_C}{12}(6m^2 + 6m + 3). \tag{3.15}$$

From this, we obtain the qubit transition frequency

$$\omega_{01} = (\sqrt{8E_J E_C} - E_C)/\hbar \tag{3.16}$$

and the anharmonicity

$$\omega_{12} - \omega_{01} = -E_C/\hbar. \tag{3.17}$$

However, the trade is a favorable one. A detailed analysis using perturbation theory shows that the decrease in sensitivity to charge noise is exponential in $\sqrt{E_J/E_C}$, while the anharmonicity only decreases linearly in $\sqrt{E_J/E_C}$ when scaled by ω_{01}. Recall that E_J/E_C can be tuned by an external magnetic flux if the Josephson junction is replaced by a SQUID.

3.4 Summary

One of the advantages of working with superconducting qubits is that we can design the electrical circuits to carry out the kind of dynamics we want. This is possible due to the fact that we can mass-produce circuit elements allowing us to test different designs to see what works best. This process is one of the key drivers of the steady advancements made in the circuits' quality and design. In fact, we might currently be relatively close to the point where the design itself is sufficient, allowing us to expand to a larger number of qubits. This advantage, though, doesn't come without a flip side. When mass-producing, no one circuit is similar at the atomic scale, which causes differences in the behavior of circuits and decoherence in the qubits. Furthermore, the usage of bulk materials carries some faults as these materials can contain impurities that then cause more decoherence in the qubits. Currently, this is just the price to pay for being able to test with different designs and compositions. There are many ways to face this problem, though, the most simple of them being better materials and enhancing the manufacturing processes. Likewise, new designs can also do their part in minimizing decoherence, and this is where modeling and simulations are key. Decoherence will, however, always be prevalent. Therefore the realistic goal is not to eliminate the decoherence but to instead minimize it so that it doesn't restrict the qubits performance excessively.

Chapter 4

Final Thoughts

4.1 Advantages over classical camputation

Used correctly, quantum computers are incredibly fast and effective. They can perform calculations in a few seconds for which today's supercomputers would need decades or even millennia. This fact is also referred to by experts as quantum superiority. For a long time, this was just a theory. In 2019, however, Google's quantum computer prototype was able to perform such a calculation and verify quantum superiority in practice. Calculations with quantum computers are particularly promising wherever incredibly complex processes with huge amounts of data are to be analyzed or simulated. In addition to digital marketing, the natural science disciplines in particular see great potential here. Quantum computers could contribute to a better and more detailed understanding of the interaction of individual particles, elements and the processes in living cells. But there are also potential applications in medicine. Quantum computing has many applications like cryptography, machine-learning, chemistry, optimisation, communication and many more. Most of all, researchers hope that quantum computers will take artificial intelligence (AI) a big step forward. These could then safely and reliably take over tasks such as data evaluation or forecasting in the future. With more engineering and scientific work to be done for necessary computation, the applications of Quantum Computing seem endless.

References

[1] Giuliano Benenti, Giulio Casati, Giuliano Strini (2004). Principles of Quantum Computation and Information, Volume I: Basic Concepts. World Scientific. ISBN: 981-238-830-3

[2] Michael A. Nielsen and Isaac L. Chuan (2010). Quantum Computation and Quantum Information. Cambridge University Press. ISBN 978-1-107-00217-3

[3] Kockum, A.F., Nori, F. (2019). Quantum Bits with Josephson Junctions. In: Tafuri, F. (eds) Fundamentals and Frontiers of the Josephson Effect. Springer Series in Materials Science, vol 286. Springer, Cham. site. `https://doi.org/10.1007/978-3-030-20726-7_17`

[4] Alexandre Zagoskin and Alexandre Blais (2008). Superconducting qubits. arXiv. `https://arxiv.org/abs/0805.0164`

[5] Wineland DJ, Monroe C, Itano WM, Leibfried D, King BE, Meekhof DM. Experimental Issues in Coherent Quantum-State Manipulation of Trapped Atomic Ions. J Res Natl Inst Stand Technol. 1998 May-Jun. site. `https://pubmed.ncbi.nlm.nih.gov/28009379/`

[6] Adriano Barenco and Charles H. Bennett and Richard Cleve and David P. DiVincenzo and Norman Margolus and Peter Shor and Tycho Sleator and John A. Smolin and Harald Weinfurter (1995). Elementary gates for quantum computation. arXiv. `https://arxiv.org/abs/quant-ph/9503016`

[7] Francesco Tafuri (2019). Fundamentals and Frontiers of the Josephson Effect. site. `https://link.springer.com/book/10.1007/978-3-030-20726-7`